

Large Eddy Simulation on the Unsteady Aerodynamics of a Heavy Duty Truck in Wind Turbulence

Prasanjit Das* and Makoto Tsubokura*

Received 29 April 2011; Accepted after revision 12 May 2011

ABSTRACT

Unsteady aerodynamic forces acting on a full-scale heavy duty truck are investigated using a large-eddy simulation technique. The numerical method adopted is first validated on a static condition measured at the DNW German-Dutch wind tunnels. After the correction of the blockage ratio in the wind tunnel, the drag coefficient obtained by our numerical method shows good agreement with the experimental data within the errors of less than 5%. Effect of an air deflector mounted on the top of a cabin is also discussed. Then the method is applied to non-stationary conditions in which the truck is subjected to ambient perturbation of approaching flow. The perturbation of the flow is a model of atmospheric turbulence and sinusoidal crosswind velocity profiles are imposed on the uniform incoming flow with its wavelength comparable to the vehicle length. As a result, it is confirmed that when the wavelength of the crosswind is close to the vehicle length, average drag increases by more than 10% and down-force decreases by about 60%, compared with the case without perturbation.

Keywords: *Large Eddy Simulation (LES), Unsteady Aerodynamics, Sinusoidal Perturbation.*

* Division of Mechanical and Space Engineering, Hokkaido University, Japan.

Email: prasanjitd11@yahoo.com

1 INTRODUCTION

In the development process of road vehicle, its aerodynamic performance is determined based on such as the aerodynamic drag or lift measured at a static condition in a wind tunnel. On the other hand, we suppose that substantial unsteady aerodynamic forces act on vehicles when they are subjected by gusty wind, abrupt maneuvering, driving over bumpy road, or overtaking. The unsteady aerodynamics is especially crucial when we would like to achieve higher driveability or safety of road vehicle. However, a precise estimation of the transient forces is difficult to measure in a wind tunnel, conventional Reynolds-averaged turbulence simulation, or even on-road testing, alternative method is strongly desired. A large-eddy simulation (LES) is a promising candidate for the solution, because it can reproduce unsteady three-dimensional turbulence structures around a vehicle or in an incoming flow. Accordingly, we have developed an unsteady aerodynamic simulator based on the High-Performance Computing (HPC) technique, which is specially designed to predict transient aerodynamic forces acting on vehicles in dynamic motion and/or in gusty wind condition [1], [2].

In this study, we focus on the effect of transient crosswind on vehicle aerodynamics. Concerning the topics, numerous experimental studies have been made so far. Among them, the wind-tunnel measurement by Beauvais in 1967 [3] is considered to be one of the pioneering works. He modified the test section of a wind tunnel by extending a track through the test section perpendicular to the main flow. Then vehicle models were mounted on the track and rushed into the test section to measure the transient aerodynamics when a vehicle encounters a wind gust. He discussed the limitation of the quasi-steady analysis in the conventional wind tunnels and pointed out that unsteady aerodynamics becomes noticeable above the yaw angle changes of 15 deg. Kobayashi and Yamada [4] also carried out an experiment to measure the transient aerodynamic forces of a one box type vehicle subjected by a wind gust. They discussed the stability of the vehicle by the yawing moment and yaw rate peak. Then the effect of windshield inclination and front end configuration on the yaw rate peak was mentioned. More recently, Dominy and Ryan [5] conducted an experiment on a generic vehicle model, using a technique where the side wind was produced by a cross jet technique. Computational Fluid Dynamics (CFD) is well developed in the automotive research field and is now a strong tool used in parallel with experiments during the design of road vehicles. Numerical approach has been

carried out by Hemida and Krajnović[6] in an attempt to investigate the transient aerodynamic response of a simplified double-deck bus in gusty winds.

Concerning the continuous yaw-angle change caused by atmospheric turbulence around vehicles, Cogotti [7] developed a turbulence generation system and mounted it on the Pininfarina wind tunnel. He investigated the effects of a turbulent flow on the aerodynamics and aeroacoustics. In these days, estimation of the effect of the transient yawing is becoming more and more important because it is strongly related to the correlation between the wind-tunnel measurements and on-road conditions. Wordley and Saunders [8] carried out on-road measurements of atmospheric turbulence at various terrains and traffic conditions and obtained the turbulence intensity and length scale of on-road turbulence. Similar on-road and wind-tunnel measurements were also done by Mayer et al. [9] they discussed the matter based on the admittance of the yawing moment. Cooper and Watkins [10] reviewed and summarized the effect of atmospheric turbulence with special focus on the application to vehicle aerodynamics. The experimental studies of Gohlke et al. [11] investigated the flow structures and forces on a 3D-bluff-body in constant cross-wind.

The effect of continuous yawing change on the aerodynamic forces is especially crucial to heavy duty trucks. The main reason is because they are used for the long distance transport and hence precise estimation of fuel consumption under cruising condition on highway subjected by atmospheric turbulence is indispensable. In addition, unexpectedly large unsteady aerodynamic force might be caused by massive flow separation at their angular corners.

Accordingly we have applied LES to a heavy duty truck to investigate the transient aerodynamic response when the vehicle is subjected by sinusoidal crosswinds. The numerical method was validated on the DNW wind tunnel data at different yaw angles between 0 to 10 deg. The vehicle was mounted on the numerical wind tunnel with the same cross-section as the experiment, and the aerodynamic drag and lateral force coefficients against the yaw were compared. Then sinusoidal perturbation was imposed in the numerical simulation, which transiently changed the relative yaw angle of the vehicle against the incoming flow from -10 to +10 deg., and unsteady aerodynamic forces acting during the process was estimated.

2 NUMERICAL METHODS

2.1 Governing Equations and Subgrid-scale Modeling

In LES, the contribution of the large, energy carrying scales to momentum and energy transfer is computed exactly, and only the effect of the unsolved small scales of the turbulence is modeled. The decomposition of the flow variable into a large scale component and a small sub-grid scale is done by applying a filtering operation:

$$\bar{f}(x_i) = \int_{\Omega} f(x'_i)G(x_i, x'_i)dx'_i \quad \dots \quad \dots \quad (1)$$

$$\frac{\partial \bar{u}_i}{\partial x_i} = 0 \quad \dots \quad \dots \quad \dots \quad (2)$$

where Ω is the entire domain, and G is the filtering function. The governing equations for the LES based on the incompressible assumption become the spatially filtered conservation equation of mass and momentum. These read, in tensor notation:

$$\frac{\partial \bar{u}_i}{\partial t} + \frac{\partial \bar{u}_i \bar{u}_j}{\partial x_j} = -\frac{\partial \bar{P}}{\partial x_i} + 2\frac{\partial}{\partial x_j}(\nu + \nu_{sgs})\bar{S}_{ij} \quad \dots \quad \dots \quad (3)$$

in which u_i , ν , and ρ are the velocity for direction, the kinetic viscosity component, and fluid density, respectively. The bar over the physical quantity indicates the spatially filtering operation for LES. The filtered strain rate tensor \bar{S}_{ij} and pressure \bar{P} in Eq.3 are expressed as,

$$\bar{S}_{ij} = \frac{1}{2} \left(\frac{\partial \bar{u}_j}{\partial x_i} + \frac{\partial \bar{u}_i}{\partial x_j} \right) \quad \dots \quad \dots \quad \dots \quad (4)$$

$$\bar{P} = \bar{p}/\rho + (\bar{u}_i \bar{u}_j - \bar{u}_i \bar{u}_j)/3 \quad \dots \quad \dots \quad \dots \quad (5)$$

The effect of subgrid-scale (SGS) turbulence on the grid-scale turbulence motion is represented by the SGS eddy viscosity, which is modeled following standard Smagorinsky [12] as

$$\nu_{sgs} = \{C_s g(l^+) \Delta\}^2 \sqrt{2\bar{S}_{ij}\bar{S}_{ij}} \quad \dots \quad \dots \quad \dots \quad (6)$$

where Δ is the volume of numerical element, and model coefficient C_s is set to be 0.15, which is generally suitable value for external flows. The damping of the turbulent effect near a wall boundary is explained by the Van-Driest type damping function as follows:

$$g(l^+) = 1 - \exp \frac{-l^+}{25} \quad \dots \quad \dots \quad \dots \quad (7)$$

where l^+ is the distance from the wall in wall coordinates.

2.2 Discretization

The spatially filtered governing equations given as **Eq.2** and **Eq.3** were discretized by a vertex-centered unstructured finite volume method. The second-order central finite difference discretization was used for the spatial derivative around the vehicle, blended with the 5% first-order upwind scheme for the convective fluxes in the Navier-Stokes equation to eliminate excessive numerical oscillation occurring on coarse and distorted tetrahedral elements. The third-order upwind scheme was adopted for the spatial derivative far away from vehicle, where coarser grid was allocated. For time marching, the third-order Adams-Moulton semi-implicit scheme was used. The SMAC (Simplified marker and cell) algorithm was employed to obtain a relationship between velocity and pressure corrections to enforce mass conservation and to obtain the pressure field. The pressure Poisson equation was solved by the incomplete Cholesky conjugate gradient (ICCG) method.

2.3 Target Vehicle Model

The configuration of the target full-scale heavy duty truck is shown in **Fig.1**. The shape was generated from the original CAD data and aerodynamically important parts such as an engine compartment under the cabin, power train components under the body, and side mirrors is reproduced, while its surface is slightly modified and simplified to fit practical CFD at reasonable computational cost. As a result, the surface of the vehicle is constructed by about 1.5 million triangle meshes. The length L , width W , and height H of the vehicle are 12.0 m, 2.5 m, and 3.7 m, respectively. To reproduce the fine structure, the surface resolution is around 5 to 10 mm around the side mirror, and relatively fine elements are allocated around the cabin. The engine and power train is reproduced by the moderate elements with the resolution of 20 to 50 mm. Larger elements are allocated to reproduce the cargo panel. The triangle element on the surface of the vehicle is indicated in **Fig.2**.

The fluid space was decomposed by tetrahedral elements. To maintain finer resolution around the vehicle, hierarchical allocation is carried out, as shown in **Fig.3**.

2. NUMERICAL METHODS

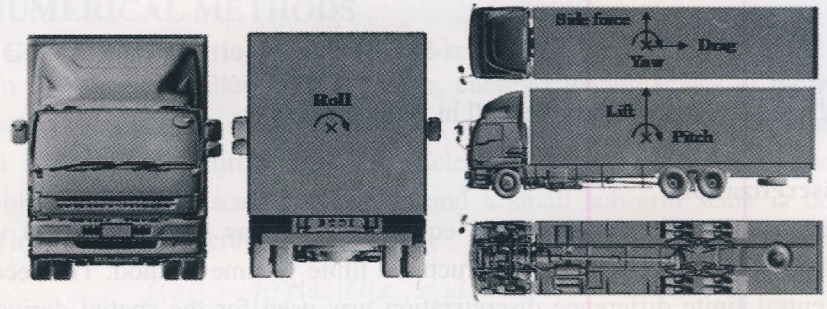


Figure 1: Full-scale heavy duty truck.

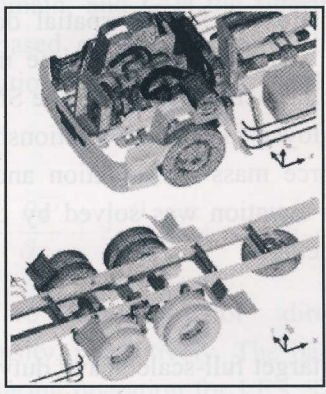


Figure 2: Space elements on the vehicle.

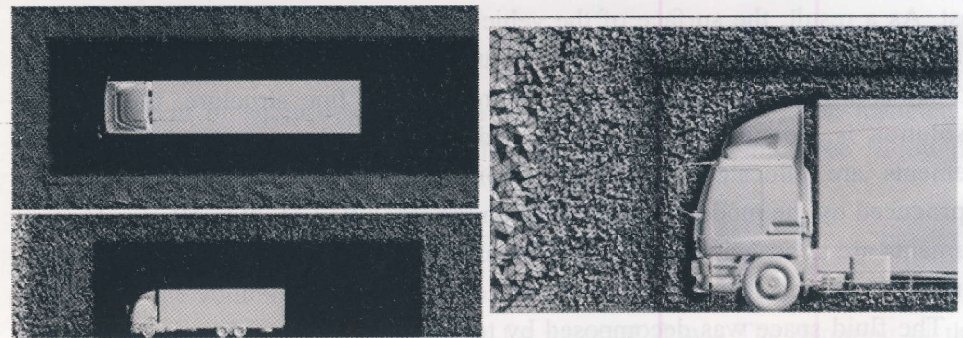


Figure 3: Space elements around the vehicle.

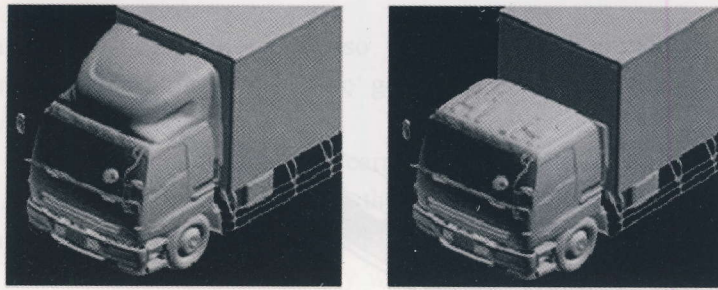
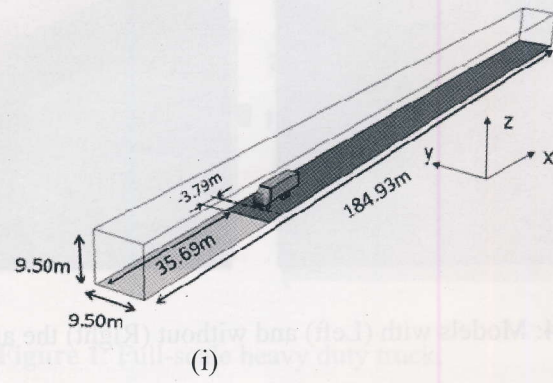


Figure 4: Models with (Left) and without (Right) the air deflector.

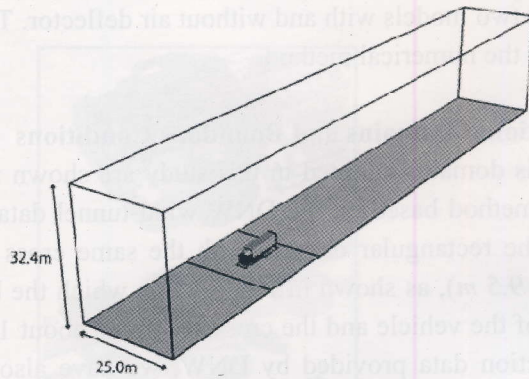
Fig.4 illustrates two models with and without air deflector. These two models are used to validate the numerical method.

2.4 Computational Domains and Boundary Conditions

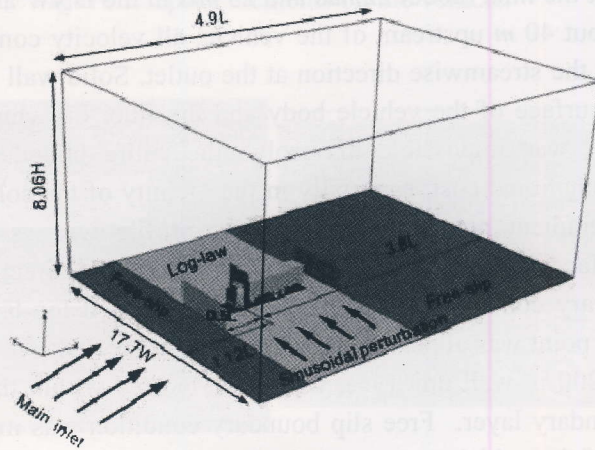
The analysis domains adopted in this study are shown in **Fig.5**. To validate our numerical method based on the DNW wind-tunnel data, the simulation was conducted on the rectangular domain with the same cross section as the wind tunnel ($9.5\text{ m} \times 9.5\text{ m}$), as shown in **Fig.5** (a), in which the blockage ratio of the projected area of the vehicle and the cross section is about 10%. To compare the blockage-correction data provided by DNW, we have also conducted the case with the blockage ratio of around 1%, as indicated in **Fig.5** (b). The case of 1% blockage is called “ideal” hereafter. In both cases, placing the uniform velocity distribution U_0 at the inlet (about 22 m/s and 25 m/s in the DNW and ideal cases, respectively) about 40 m upstream of the vehicle, all velocity components were gradient-free for the streamwise direction at the outlet. Solid wall condition was adopted on the surface of the vehicle body and the floor on which the vehicle was mounted. It was impossible to resolve the entire boundary layer at a reasonable computational cost, especially in the vicinity of the solid wall where large velocity gradient appears. Thus log-law profile was assumed on the velocity and surface friction on the wall was estimated and directly imposed as Neumann boundary condition. As a result of the assumed log-law profile, the first nearest grid point was allocated so as to maintain the distance from the wall less than about 200 in wall unit (y^+), which are located within the logarithmic layer of the boundary layer. Free slip boundary condition was imposed on the floor upstream of the vehicle to prevent the boundary layer from developing on the ground. In the DNW case in **Fig.5** (a), the exit of the wind tunnel nozzle is located 3.79 m windward of the vehicle. The side walls, unless otherwise stated,



(i)

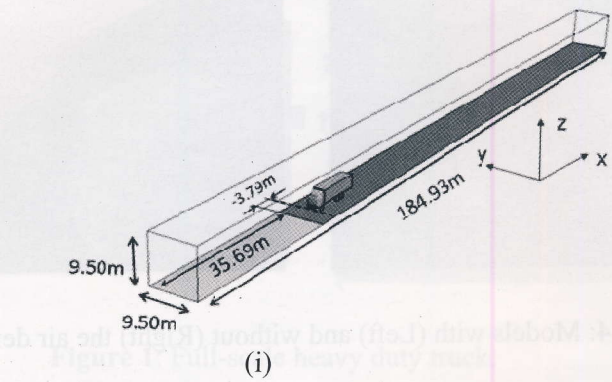


(ii)

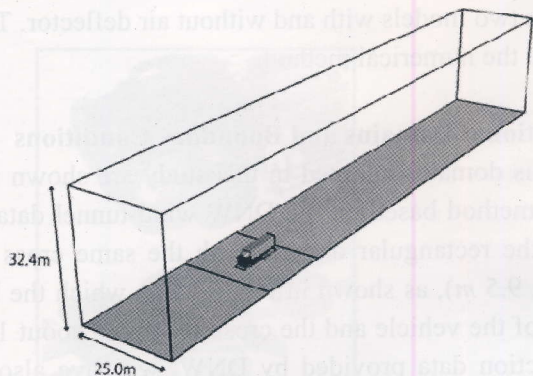


(iii)

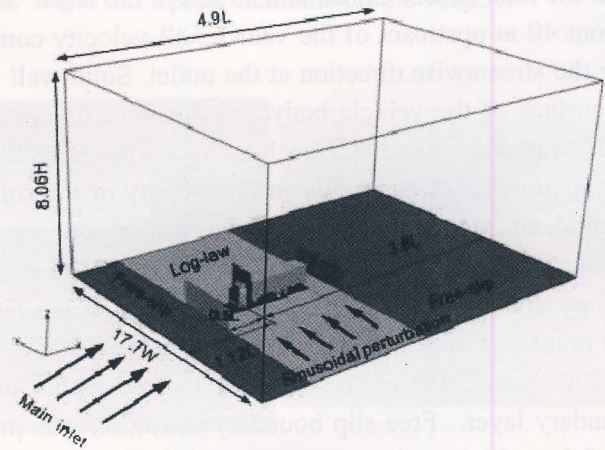
Figure 5: Computational domains: (i) DNW, (ii) ideal and (iii) sinusoidal crosswind.



(i)



(ii)



(iii)

Figure 5: Computational domains: (i) DNW, (ii) ideal and (iii) sinusoidal crosswind.

and ceiling of the domain were also treated as slip boundary, where grid resolution normal to the walls were generally so coarse that capturing the boundary layer is out of scope.

The crosswind simulation was carried out in the domain illustrated in **Fig.5 (c)**. The model was mounted on the floor of the rectangular domain, with its length, width, and height given as $4.9L$, $17.7L$, and $8.06H$. The blockage ratio was less than 0.7%. The inlet velocity was set to 25 m/s . In the simulation, the unsteady aerodynamic around the vehicle was obtained by the superimposed of sinusoidal transverse perturbation on the inlet incoming flow. The unsteady sinusoidal perturbations were imposed as an inlet/outlet boundary condition on both sides of the computational domain.

3 RESULTS AND DISCUSSION

3.1 Validation of the Numerical Method

The numerical method was validated by comparing the drag and side forces obtained with the DNW wind-tunnel data provided. Three yaw angles of 0, 5, and 10 deg. with respect to the incoming flow were considered. Two models with and without the air deflector are compared here. As noted in the previous section, the ideal data based on the experimental measurements were obtained by considering the blockage correction equation proposed by DNW. The corresponding LES results in the ideal case were obtained in the domain with larger cross section (1% blockage).

The errors of the LES results with respect to the experimental data are summarized in **Table.1** and **Table.2**. It should be reminded here that we have used exactly the same spatial resolution around the vehicle for all cases, thus the numerical error included in the results is exactly the same. For the model with the air deflector, the LES underestimates the drag in the DNW condition by about 10%, as shown in **Table.1**. In the same way, the LES underestimates the drag in the model without the air deflector in the DNW geometry, while its underestimation varies from -10 to -17% depending on the yawing angle, as indicated in **Table.2**. The underestimation is mitigated in the "ideal" condition, and the error is less than 5% for the model with the air deflector.

On the other hand, for the model without the air deflector, the errors in the ideal condition varies from -1.3% to -7% strongly depending on the yawing angle. The corresponding normalized drag coefficient by the value at the yaw of

TABLE 1: Drag coefficient (above) and lateral force (below) errors against DNW wind-tunnel data for the model with the air deflector

β Yaw angle (degrees)	0	5	10
Cd errors against DNW data (%)	-8.2	-10	-9.5
Cd errors against Ideal data (%)	-3.3	-4.5	-3.3
β Yaw angle (degrees)	0	5	10
Cs errors against DNW data (%)	negligible	-9.7	-5.3
Cs errors against Ideal data (%)	negligible	-10	-5.4

TABLE 2: Drag coefficient (above) and lateral force (below) errors against DNW wind-tunnel data for the model without the air deflector

β Yaw angle (degrees)	0	5	10
Cd errors against DNW data (%)	-9.7	-12	-17
Cd errors against Ideal data (%)	-1.3	-4.1	-7
β Yaw angle (degrees)	0	5	10
Cs errors against DNW data (%)	negligible	-15	-12.7
Cs errors against Ideal data (%)	negligible	-9.3	-3.7

0 deg is shown in **Fig.6**. Concerning the relatively large discrepancies in the DNW geometry, the possible explanation is the difference of the duct configuration before and after the test section between CFD and the DNW. As indicated in **Fig.5**, we treat the duct as a simple rectangular shape in the simulation, while in the DNW, the test section on which the vehicle is mounted is about 20 m length and the nozzle and diffuser are mounted before and after the section. Because of the relatively short test section with respect to wake length of the vehicle, the drag is more or less affected by the stream-wise pressure gradient in the diffuser.

Other important thing to be noted is the dependence of the error on the yawing angle in the case of the model without air deflector. In Europe, the air

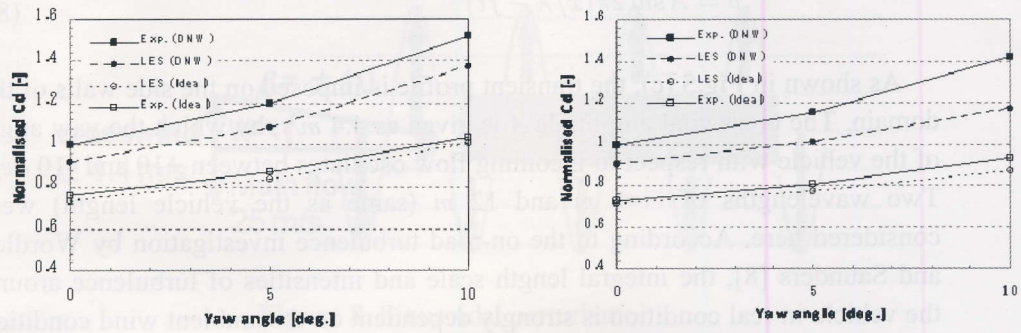


Figure 6: Normalized drag coefficient for the models with (Left) and without (Right) the air the air deflector.

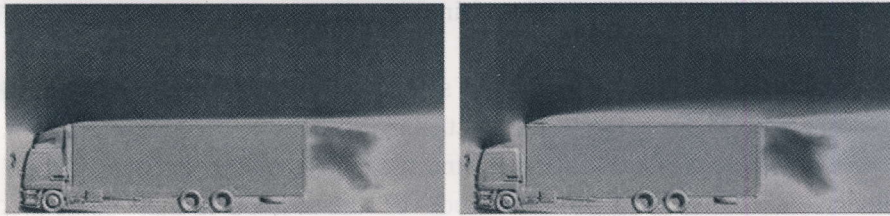


Figure 7: Mean streamwise velocity distribution on the central cross section. Contours between -10 to 30 m/s, Left, with the air deflector; Right, without the air deflector.

deflector is commonly used as a standard model, thus the blockage correction of the drag in the DNW is mainly tuned based on the model with the deflector.

While in the model without the deflector, the flow above the cabin is perturbed by the large separation in front of the cargo (as shown in Fig.7), and the separated flow is strongly affected by the yawing angle. Thus it is reasonable to say that other blockage correction than the one tuned on the air deflector model should be developed for the proper correction on the model without deflector. Finally, it should be noted that the effect of drag reduction by the air deflector identified in the wind-tunnel experiment is 16.5%, while that in the LES is 15%, indicating that accuracy of our LES is satisfactory.

3.2 Sinusoidal Crosswind Perturbation

The model with the air deflector was used for the numerical investigation of the effect of sinusoidal crosswind perturbation. The sinusoidal crosswind profile imposed on the uniform main flow is given by

$$v = A \sin 2\pi(x/\lambda - ft) \quad \dots \quad \dots \quad \dots \quad (8)$$

As shown in **Fig.5** (c), the transient profile is imposed on the side walls of the domain. The crosswind amplitude A is given as 4.4 m/s , by which the yaw angle of the vehicle with respect to incoming flow oscillates between $+10$ and -10 deg . Two wavelengths of $\lambda=6 \text{ m}$ and 12 m (same as the vehicle length) were considered here. According to the on-road turbulence investigation by Wordley and Saunders [8], the integral length scale and intensities of turbulence around the vehicle in real condition is strongly dependent on the ambient wind condition on the road. The maximum length was observed in smooth terrain around 24 m , with turbulence intensities about 1 to 5% and in the city canyon, the integral length scale around 15 m .

The minimum length was found in a freeway traffic condition about 6 m , while its turbulence intensity up to 16% . In all cases, the length scale is comparable to the vehicle length. By setting the frequency $f = U_0/\lambda$, in which $U_0 = 25 \text{ m/s}$ is the main-flow velocity, the sinusoidal wave travels with the same speed as the main flow. Then the sinusoidal perturbation is imposed on the vehicle, which is fixed on the floor of the computational domain. The corresponding sinusoidal perturbation frequency measured on the vehicle becomes 2.08 Hz and 4.16 Hz at $\lambda=12 \text{ m}$ and 6 m , respectively.

The schematic view of the sinusoidal transversal velocity profile imposed on the vehicle, together with the relationship of its amplitude, incoming flow velocity, and yaw angle is shown in **Fig.8**. Hereafter, the yaw angle β of the vehicle with respect to the incoming flow is defined at the leading end of the vehicle.

A lateral view of the crosswind velocity profiles when the vehicle is subjected to the sinusoidal perturbation is shown in **Fig.9**. The decay of the crosswind velocity about 30 m above the vehicle in the case of $\lambda=6 \text{ m}$ is identified, which is due to the coarser grid allocation around that region, while supposed crosswind profiles are properly imposed around the vehicle.

The trajectories of the phase-averaged drag, lateral, and lift against the relative yaw angle β are depicted in **Fig.10**, where arrow indicates the direction of trajectory motion. The static aerodynamics forces measured at fixed yaw angle of 0 , 5 , and 10 deg . at the corresponding relative incoming velocity are also plotted for better understanding the difference between the transient and the quasi-steady analysis.

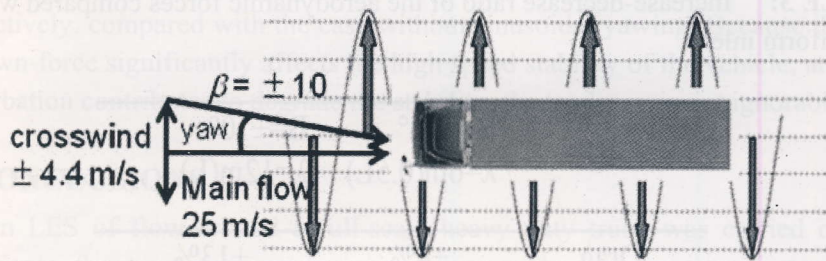


Figure 8: Sinusoidal perturbation.

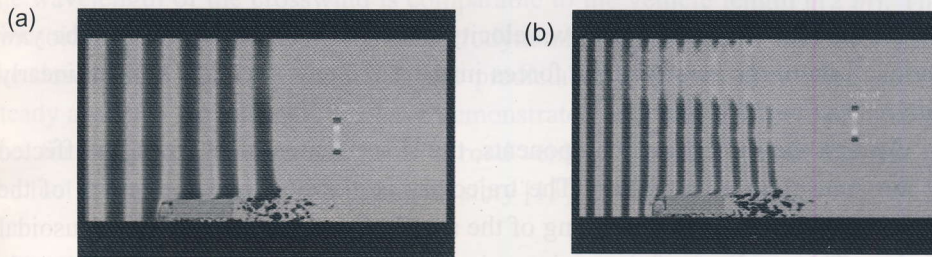


Figure 9: Lateral view of the crosswind velocity profiles: (a) $\lambda = 12\text{ m}$ and (b) $\lambda = 6\text{ m}$.

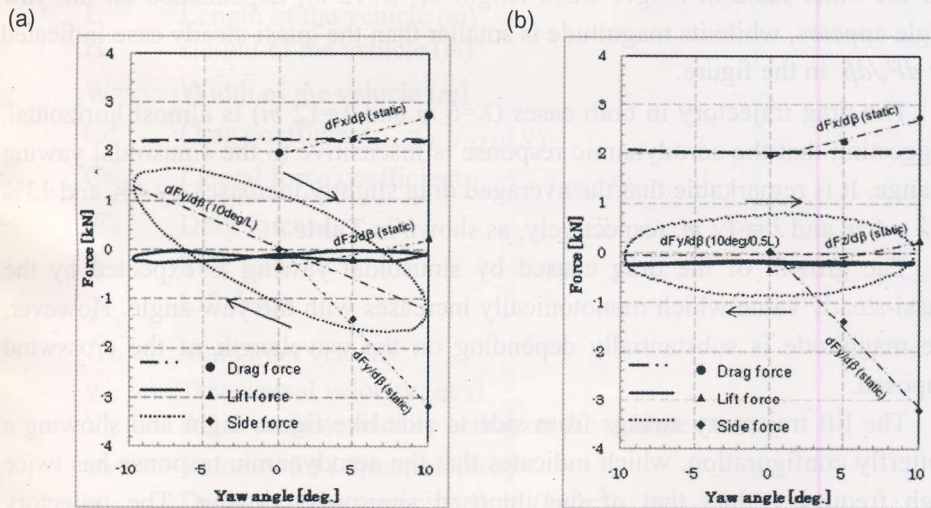


Figure 10: Trajectory of phase-averaged aerodynamic forces (a) $\lambda = 6\text{ m}$ and (b) $\lambda = 12\text{ m}$.

TABLE 3: Increase-decrease ratio of the aerodynamic forces compared with the uniform inlet.

Force	B=±10° λ=6m(0.5L)	B=±10° λ=12m(L)
Drag	+4%	+13%
Lift	-37%	-60%

As the relative incoming flow velocity increases with an increase in the yaw angle, all the three aerodynamic forces in the static case increase almost linearly with respect to the yaw angle.

Among the three force components, the side force is most strongly affected by the sinusoidal perturbation. The trajectory is elliptical and the length of the minor axis indicates phase shifting of the aerodynamic response to the sinusoidal yawing. The gradient of the major axis represents the dependence of the side force on the yaw angle. In the shorter wavelength case at $\lambda = 6 m$, the trajectory is horizontal, thus suggesting that the side force is independent on the yaw angle and effect of the transient yawing appears as only phase shifting of the response. On the other hand at longer wave length of $\lambda=12 m$, dependence on the yaw angle appears, while its magnitude is smaller than the quasi-steady case indicated by $dF_x/d\beta$ in the figure.

The drag trajectory in both cases ($\lambda=6 m$ and $\lambda=12 m$) is almost horizontal, suggesting that the aerodynamic response is insensitive to the sinusoidal yawing change. It is remarkable that the averaged drag slightly increases by 4% and 13% at $\lambda = 6 m$ and $\lambda = 12 m$, respectively, as shown in **Table.3**.

The growth of the drag caused by sinusoidal yawing is expected by the quasi-steady value which monotonically increases with the yaw angle. However, the magnitude is substantially depending on the wavelength of the crosswind imposed.

The lift trajectory swings from side to side like figure eight and showing a butterfly configuration, which indicates that the aerodynamic response has twice high frequency than that of the imposed sinusoidal yawing. The trajectory becomes wider for the vertical direction at longer wavelength. Owing to the transient yawing, the down-force decreases by 37% and 60% at $\lambda=6 m$ and $12 m$,

respectively, compared with the case without sinusoidal yawing. Because the lift or down-force significantly affects the high speed stability of the vehicle, and the perturbation contributes to degrade the stability, the tendency is not ignorable.

4 CONCLUSIONS

An LES of flow around a full-scale heavy duty truck was carried out to investigate the transient aerodynamic forces under the continuous transient yawing. At the condition of sinusoidal yawing with the amplitude of -10 to 10 deg., averaged drag and lift are substantially affected by the perturbation when the wavelength of the crosswind is comparable to the vehicle length (12 m). The sinusoidal perturbation increases the aerodynamic drag by 13 % and decreases the down-force by 60 %, which is not predictable by the conventional quasi-steady analysis. Accordingly we have demonstrated that LES will be a promising tool for the aerodynamic assessment of road vehicle, especially in the context of the fuel consumption, driveability, and safety [13], [14].

NOMENCLATURES

A	Amplitude of the sinusoidal crosswind velocity (<i>m</i>)
S	Frontal area of the vehicle (<i>m</i> ²)
C	Cross-sectional area of wind tunnel test section
L	Length of the vehicle (<i>m</i>)
H	Height of the vehicle (<i>m</i>)
W	Width of the vehicle (<i>m</i>)
C _d	Drag coefficient ($= 2 F_x / \rho U_0^2 S$)
C _s	Lateral force coefficient ($= 2 F_y / \rho U_0^2 S$)
<i>F_x</i>	Drag force
<i>F_y</i>	Side force
<i>F_z</i>	Lift force
<i>U</i> ₀	Main inlet velocity
<i>v</i>	Transversal velocity (<i>m/s</i>)
<i>V</i> ₀	Relative flow velocity acting on the vehicle (<i>m/s</i>)
<i>u_i</i>	Velocity for <i>i</i> direction (<i>m/s</i>)
ρ	Density of the incoming fluid (<i>kg/m</i> ³)
<i>x, y, z</i>	Main streamwise, transversal, vertical

ACKNOWLEDGMENTS

This work is supported by the Industrial Technology Research Grant Program in 2007 from New Energy and Industrial Technology Development Organization (NEDO) of Japan. A portion of this research was also supported by the grant for "Strategic Program—Preliminary Research Field No. 4: Industrial Innovations" from the Ministry of Education, Culture, Sports, Science, and Technology (MEXT)'s "Development and Use of Advanced, High-Performance, General-Purpose Supercomputers Project," and carried out in partnership with the University of Tokyo. This research was carried out in a collaborative research project with Isuzu Advanced Engineering Center Ltd., and the geometry data and experimental data received are greatly acknowledged.

REFERENCES

- [1] Tsubokura M, Nakashima T, Ikenaga T, Onishi K, Kitoh K, Oshima N, and Kobayashi T. (2008) HPC- LES for the prediction of unsteady aerodynamic forces on a vehicle in a gusty cross-flow condition. *SAE Motorsports Engineering Conference*, SAE paper No. 2008-01-3001.
- [2] Tsubokura M, Nakashima T, Kitoh K, Sasaki Y, Oshima N, and Kobayashi T. (2009) Development of an unsteady aerodynamic simulator using large-eddy simulation based on high-performance computing technique. *SAE International journal of passenger cars – Mechanical systems*, Vol. 2(1): pp.168-178.
- [3] Beauvais FN. (1967) Transient nature of wind gust effects on an automobile. *SAE paper* No. 670608.
- [4] Kobayashi N and Yamada M. (1988) Stability of a one box type vehicle in a cross-wind -An analysis of transient aerodynamic forces and moments. *SAE paper* No. 881878.
- [5] Dominy RG and Ryan A. (1999) An Improved Wind Tunnel Configuration for the Investigation of Aerodynamic Cross Wind Gust Response. *SAE Paper* No. 1999-01-0808.
- [6] Hemida H and Krajinović S. (2009) Transient Simulation of the Aerodynamic Response of Double-Deck Bus in Gusty Winds. *J. of Fluids Eng., Trans. ASME*, Vol. 131: pp. 031101-1-10.

- [7] Cogotti A. (2003) Generation of a controlled level of turbulence in the Pininfarina wind tunnel for the measurement of unsteady aerodynamics and aeroacoustics. *SAE Paper* No. 2003-01-0430.
- [8] Wordley S and Saunders J. (2009) On-road turbulence: part2. *SAE Paper* No. 2009-01-0002.
- [9] Mayer J, Schrefl M and Demuth R. (2007) On various aspects of the unsteady aerodynamic effects on cars under crosswind conditions. *SAE Paper* No. 2007-01-1548.
- [10] Cooper KR and Watkins S. (2007) The unsteady wind environment of road vehicles, Part one: A review of the on-road turbulent wind environment. *SAE Paper* No. 2007-01-1236.
- [11] Gohlke M, Beaudoin JF, Amielh M and Anselmet F. (2007) Experiment analysis of flow structures and forces on a 3D-bluff-body in constant cross-wind. *Exp Fluids*, Vol. 43: pp. 579-594.
- [12] Smagorinsky J. (1963) General Circulation Experiments with the Primitive Equations, 1. The Basic Experiment. *Monthly Weather Rev.*, Vol. 91, No. 3: pp. 99-164.
- [13] Tsubokura M, Kobayashi T, Nakashima T, Nouzawa T, Nakamura T, Zhang H, Onishi K and Oshima N. (2009) Computational visualization of unsteady flow around vehicles using high performance computing. *Computers & Fluids*, Vol.38: pp.981-990.
- [14] Tsubokura M, Nakashima T, Kitayama M, Ikawa Y, Doh DH and Kobayashi T. (2010) Large eddy simulation on the unsteady aerodynamic response of a road vehicle in transient crosswinds. *Int. J. of Heat and Fluid Flow*, Vol.31: pp.1075-1086.

1. Papers submitted for publication will be referred to the listed reviewers for assessment. However, the editorial board will make initial screening of the papers.
2. After the assessment, the authors may be requested to modify/clarify certain points.
3. Accepted/modified/corrected papers will be published in the next issue of the Journal.

(Contd. from 2nd cover page)

8. SI units must be used in the manuscript. However, other units may be used in parenthesis.
9. Tables should be referred to in consecutive Arabic numerical. Each table must have a table caption.
10. Line drawings must be in a form suitable for reproduction e.g., laser printout, drawn in Indian ink on white paper or on tracing paper. Photographs should have a glossy finish. Each figure must have a number and a figure caption. Electronic mode is preferred.
11. References should be set out in alphabetical order of the author's last name in a list at the end of the article. They should be given in standard form as in the following examples :
 - (a) Journal
Bloomer G and Wright A. (1984) Scheduling of Vehicles from Factory to Depot. *Journal of Vehicles*, Vol. 12: pp. 590-598.
 - (b) Book
Best, John., and Kahn, James V., Research in Education, Prentice-Hall, New Jersey, 1986.
 - (c) Monograph
Syedali, M.M. "Computer Controlled Car", Thesis, M.Sc. Engineering, Department of Mechanical Engineering, BUET, 1990
 - (d) Conference Paper
Hasan M and Ullah MS. "Tourism development in the Chittagong Hill Tracts of Bangladesh after the peace agreement of 1997", a paper submitted to the Regional Conference on physical mobility and

development in the mountains", Tribhuvan University, 15-17, March, 2000 Kathmandu, Nepal, pp.12

- (e) Unpublished paper
Ahmadi, R and Tangs : Production Allocation with Dual Provisioning, Working Paper, Anderson Graduate School of Management, UCLA (1991)
 12. The University does not accept responsibility for loss or damage of manuscript while in mail.
 13. The responsibility for opinions in the contributions rests entirely on their authors.
 14. The author (s) must submit declaration that the paper was not published elsewhere.
 15. In case of joint papers, communication will be made with the first author.
 16. The University will reserve the copyright of the paper once it is accepted for publication in the Journal. The authors must obtain written permission from REASP, IUT for publication elsewhere.
- Procedure for acceptance of papers and publications :
1. Papers submitted for publication will be referred to the listed reviewers for assessment. However, the editorial board will make initial screening of the papers.
 2. After the assessment, the authors may be requested to modify/clarify certain points.
 3. Accepted/modified/corrected papers will be published in the next issue of the Journal.